

Bayesian inference of ODEs with Gaussian processes

Pashupati Hegde

Çağatay Yıldız

Harri Lähdesmäki

Samuel Kaski

Markus Heinonen

Department of Computer Science
Aalto University, Finland
first.last@aalto.fi

Abstract

Recent machine learning advances have proposed black-box estimation of *unknown continuous-time system dynamics* directly from data. However, earlier works are based on approximative ODE solutions or point estimates. We propose a novel Bayesian nonparametric model that uses Gaussian processes to infer posteriors of unknown ODE systems directly from data. We derive sparse variational inference with decoupled functional sampling to represent vector field posteriors. We also introduce a probabilistic shooting augmentation to enable efficient inference from arbitrarily long trajectories. The method demonstrates the benefit of computing vector field posteriors, with predictive uncertainty scores outperforming alternative methods on multiple ODE learning tasks.

1 Introduction

Ordinary differential equations (ODEs) are powerful models for continuous-time non-stochastic systems, which are ubiquitous from physical and life sciences to engineering (Hirsch et al., 2012). In this work, we consider non-linear ODE systems

$$\mathbf{x}(t) = \mathbf{x}_0 + \int_0^t \mathbf{f}(\mathbf{x}(\tau)) d\tau, \quad \dot{\mathbf{x}}(t) := \frac{d\mathbf{x}(t)}{dt} = \mathbf{f}(\mathbf{x}(t)), \quad (1)$$

where the state vector $\mathbf{x}(t) \in \mathbb{R}^D$ evolves over time $t \in \mathbb{R}_+$ from an initial state \mathbf{x}_0 , following its time derivative $\dot{\mathbf{x}}(t)$. Our goal is to learn the differential function $\mathbf{f} : \mathbb{R}^D \mapsto \mathbb{R}^D$ from state observations, when the functional form \mathbf{f} is unknown.

The conventional mechanistic approach involves manually defining the equations of dynamics and optimizing their parameters (Butcher and Goodwin, 2008) or inferring their posteriors (Girolami, 2008) from data. However, the equations are unknown or ambiguous for many systems, such as human motion (Wang et al., 2008). Early seminal works explored fitting unknown ODEs with splines (Henderson and Michailidis, 2014), Gaussian processes (Äijö and Lähdesmäki, 2009) or kernel methods (Heinonen and d’Alché-Buc, 2014) by resorting to biased gradient matching approximations (Varah, 1982). Recently, accurate estimation of free-form non-linear dynamics was proposed using Gaussian processes with sensitivity equations (Heinonen et al., 2018) and neural networks with adjoints (Chen et al., 2018). However, both approaches are restricted to learning point estimates of the dynamics, limiting their uncertainty characterization and generalization.

In this work, we introduce Bayesian learning of unknown, non-linear ODEs. Our contributions are:

- We use Gaussian processes as flexible priors over differentials \mathbf{f} , and propose stochastic variational inference to learn posteriors over vector fields.

- We adapt decoupled functional sampling to simulate ODEs in linear time from vector field posteriors.
- For the difficult problem of vanishing gradients, which renders straightforward solutions useless on long trajectories, we introduce a novel probabilistic shooting method. It is motivated by the canonical shooting methods from optimal control and makes inference stable and efficient on long trajectories.
- We empirically show the effectiveness of our method even while learning from a limited number of observations. We demonstrate the ability to infer arbitrarily long trajectories efficiently with the shooting extension.

2 Related works

Mechanistic ODE models. In mechanistic modelling the equation \mathbf{f}_θ is predefined with a set of coefficients θ to be fitted (Butcher and Goodwin, 2008). Several works have proposed embedding mechanistic models within Bayesian or Gaussian process models (Calderhead et al., 2008; Dondelinger et al., 2013; Macdonald et al., 2015). Recently both Julia and Stan have introduced support for Bayesian analysis of parametric ODEs (Rackauckas and Nie, 2017; Stan, 2021).

Free-form ODE models. Multiple works have proposed fitting unknown, non-linear and free-form ODE differentials with gradient matching (Ramsay et al., 2007) using splines (Henderson and Michailidis, 2014), Gaussian processes (Äijö and Lähdesmäki, 2009; Äijö et al., 2013; Ridderbusch et al., 2020; Wenk et al., 2020) or kernel methods (Heinonen and d’Alché-Buc, 2014). Recently, Heinonen et al. (2018) proposed accurate maximum a posteriori optimisation of vector fields with sensitivity equation gradients (Kokotovic and Heller, 1967). Neural ODEs (Chen et al., 2018) introduced adjoint gradients (Pontryagin et al., 1962) along with flexible black-box neural network vector fields. Several extensions to learning latent ODEs have been proposed (Yildiz et al., 2019; Rubanova et al., 2019). Bhourri and Perdikaris (2021) proposes a hybrid model combining neural networks and Gaussian processes for sparse ODE system discovery (Brunton et al., 2016).

Discrete-time state-space models. There is a large literature on Markovian state-space models that operate over discrete time increments (Wang et al., 2005; Turner et al., 2010; Frigola et al., 2014). Typically nonlinear state transition functions are model with Gaussian processes and applied to latent state estimation or system identification problems with dynamical systems (Eleftheriadis et al., 2017; Doerr et al., 2018; Ialongo et al., 2019). This paper will focus on continuous-time models and leave the study of discrete vs. continuous formulations for future work.

Method	ODE posterior	Freeform dynamics	Exact gradients	Reference
NeuralODE	✗	✓	✓	Chen et al. (2018)
npODE	✗	✓	✓	Heinonen et al. (2018)
Gradient matching	✗	✓	✗	Ramsay et al. (2007); Heinonen and d’Alché-Buc (2014)
Mechanistic GM	✓	✗	✗	Dondelinger et al. (2013); Wenk et al. (2020)
GPODE	✓	✓	✓	this work

Table 1: Related work: for each method, we indicate if it can learn posterior over vector fields, does it assume an unknown system dynamics, and whether the inference is performed directly over the observations or on the empirical gradients

3 Methods

We consider the problem of learning ODEs (1) and propose a Bayesian model to infer posteriors over the differential $\mathbf{f}(\cdot)$.

3.1 Bayesian modeling of ODEs using GPs

We assume a sequence of N observations $\mathbf{Y} = (\mathbf{y}_1, \mathbf{y}_2, \dots, \mathbf{y}_N)^T \in \mathbb{R}^{N \times D}$, with $\mathbf{y}_i \in \mathbb{R}^D$ representing the noisy observation of the unknown state $\mathbf{x}(t_i) \in \mathbb{R}^D$ at time t_i . We assume a zero

mean vector-valued Gaussian process prior over \mathbf{f} ,

$$\mathbf{f}(\mathbf{x}) \sim \mathcal{GP}(\mathbf{0}, K(\mathbf{x}, \mathbf{x}')), \quad (2)$$

which defines a distribution of functions $\mathbf{f}(\mathbf{x})$ with covariance $\text{cov}[\mathbf{f}(\mathbf{x}), \mathbf{f}(\mathbf{x}')] = K(\mathbf{x}, \mathbf{x}')$, where $K(\mathbf{x}, \mathbf{x}') \in \mathbb{R}^{D \times D}$ is a matrix-valued kernel (Alvarez et al., 2012).

$$p(\mathbf{U}) = \mathcal{N}(\mathbf{U}|\mathbf{0}, \mathbf{K}_{\mathbf{ZZ}}) \quad (3)$$

$$p(\mathbf{f}|\mathbf{U}; \mathbf{Z}) = \mathcal{N}(\mathbf{f}|\mathbf{A}\text{vec}(\mathbf{U}), \mathbf{K}_{\mathbf{XX}} - \mathbf{A}\mathbf{K}_{\mathbf{ZZ}}\mathbf{A}^T), \quad (4)$$

where $\mathbf{X} = (\mathbf{x}_1, \mathbf{x}_2, \dots, \mathbf{x}_{N'})^T \in \mathbb{R}^{N' \times D}$ collects all the intermediate state evaluations $\mathbf{x}(t_i)$ encountered along numerical approximation of the true continuous ODE integral (1), $\mathbf{f} = (\mathbf{f}(\mathbf{x}_1)^T, \dots, \mathbf{f}(\mathbf{x}_{N'})^T)^T \in \mathbb{R}^{N'D \times 1}$, $\mathbf{K}_{\mathbf{XX}}$ is a block-partitioned matrix of size $N'D \times N'D$ with $D \times D$ blocks, so that block $(\mathbf{K}_{\mathbf{XX}})_{i,j} = K(\mathbf{x}_i, \mathbf{x}_j)$, and $\mathbf{A} = \mathbf{K}_{\mathbf{XZ}}\mathbf{K}_{\mathbf{ZZ}}^{-1}$. For notational simplicity, we assume that the measurement time points are among the time points of the intermediate state evaluations.

The joint probability distribution follows

$$p(\mathbf{Y}, \mathbf{f}, \mathbf{U}, \mathbf{x}_0) = p(\mathbf{Y}|\mathbf{f}, \mathbf{x}_0)p(\mathbf{f}, \mathbf{U})p(\mathbf{x}_0) = \prod_{i=1}^N \underbrace{p(\mathbf{y}_i|\mathbf{f}, \mathbf{x}_0)}_{\text{likelihood}} \underbrace{p(\mathbf{f}|\mathbf{U})p(\mathbf{U})}_{\text{GP prior}} \underbrace{p(\mathbf{x}_0)}_{\text{state prior}}, \quad (5)$$

where the conditional distribution $p(\mathbf{y}_i|\mathbf{f}, \mathbf{x}_0) = p(\mathbf{y}_i|\mathbf{x}_i)$ computes the likelihood over ODE state solutions $\mathbf{x}_i = \mathbf{x}_0 + \int_0^{t_i} \mathbf{f}(\mathbf{x}(\tau))d\tau$ for a single realization of vector field $\mathbf{f} \sim p(\mathbf{f})$ and the initial state $\mathbf{x}_0 \sim p(\mathbf{x}_0)$.

3.2 Variational inference for GP-ODEs

In contrast to earlier approaches that estimate MAP solutions (Heinonen et al., 2018; Ridderbusch et al., 2020), our goal is to infer the posterior distribution $p(\mathbf{f}, \mathbf{x}_0|\mathbf{Y})$ of the vector field \mathbf{f} and initial value \mathbf{x}_0 from observations \mathbf{Y} . The posterior is intractable due to the non-linear integration map $\mathbf{x}_0 \mapsto \mathbf{x}(t)$.

We propose the stochastic variational inference framework (SVI) (Titsias, 2009; Hensman et al., 2013) for sparse GP-based ODE modelling. We introduce a factorized Gaussian posterior approximation for the inducing variables across state dimensions $q(\mathbf{U}) = \prod_{d=1}^D \mathcal{N}(\mathbf{u}_d|\mathbf{m}_d, \mathbf{Q}_d)$, $\mathbf{u}_d \in \mathbb{R}^M$ where $\mathbf{m}_d \in \mathbb{R}^M$, $\mathbf{Q}_d \in \mathbb{R}^{M \times M}$ are the mean and covariance parameters of the variational Gaussian posterior approximation for the inducing variables. We treat the inducing locations \mathbf{Z} as optimized hyperparameters¹. The posterior distribution for the variational approximation is then

$$q(\mathbf{f}) = \int p(\mathbf{f}|\mathbf{U})q(\mathbf{U})d\mathbf{U} \quad (6)$$

$$= \int \underbrace{\mathcal{N}(\mathbf{f}|\mathbf{A}\text{vec}(\mathbf{U}), \mathbf{K}_{\mathbf{XX}} - \mathbf{A}\mathbf{K}_{\mathbf{ZZ}}\mathbf{A}^T)}_{\text{interpolation}} \underbrace{q(\mathbf{U})}_{\text{inducing}} d\mathbf{U}. \quad (7)$$

The posterior inference goal then translates to estimating the posterior $p(\mathbf{U}, \mathbf{x}_0|\mathbf{Y})$ of the inducing points \mathbf{U} and initial state \mathbf{x}_0 . Under variational inference the learning objective translates into

¹See Rossi et al. (2021) for discussion on inducing locations inference.

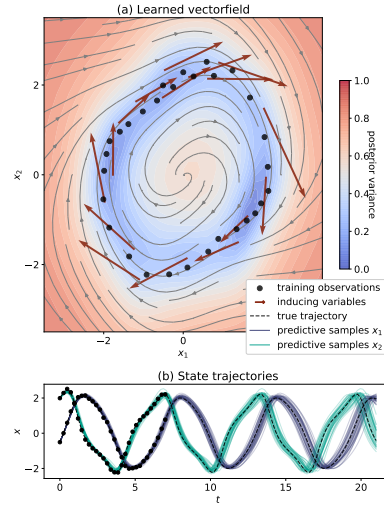


Figure 1: Illustration of GPODE: The model learns a GP posterior (a) of a vector field. Valid ODE trajectories are sampled from the posterior process as shown in (b).

maximizing the evidence lowerbound (ELBO) (Blei et al., 2017),

$$\log p(\mathbf{Y}) \geq \sum_{i=1}^N \underbrace{\mathbb{E}_{q(\mathbf{f}, \mathbf{x}_0)} \log p(\mathbf{y}_i | \mathbf{f}, \mathbf{x}_0)}_{\text{variational likelihood}} - \underbrace{\text{KL}[q(\mathbf{U}) || p(\mathbf{U})]}_{\text{inducing KL}} - \underbrace{\text{KL}[q(\mathbf{x}_0) || p(\mathbf{x}_0)]}_{\text{initial state KL}} =: \mathcal{L}, \quad (8)$$

where we also assume posterior approximation $q(\mathbf{x}_0) = \mathcal{N}(\mathbf{a}_0, \Sigma_0)$ for the initial state \mathbf{x}_0 .

3.3 Sampling ODEs from Gaussian processes

The Picard-Lindelöf theorem (Lindelöf, 1894) requires valid ODE systems to define unique solutions to the initial value problem (IVP) (1). Our goal is to efficiently sample GP functions $\mathbf{f}(\cdot) \sim q(\mathbf{f})$ (7), such that we can evaluate the sample function $\mathbf{f}(\mathbf{x}(t))$ at arbitrary states $\mathbf{x}(t)$ encountered during ODE forward integration, while accounting for both the inducing and interpolation distributions of Equation (7). Function-space sampling of such GPs has prohibitive cubic complexity (Rasmussen and Williams, 2006; Ustyuzhaninov et al., 2020), while the more efficient weight-space sampling with Fourier bases cannot express the posterior (7) non-stationarity (Wilson et al., 2020).

We use the decoupled sampling that decomposes the posterior into two parts (Wilson et al., 2020),

$$\underbrace{\mathbf{f}(\mathbf{x}) | \mathbf{U}}_{\text{posterior}} = \underbrace{\mathbf{f}(\mathbf{x})}_{\text{prior}} + \underbrace{K(\mathbf{x}, \mathbf{Z})K(\mathbf{Z}, \mathbf{Z})^{-1}(\mathbf{U} - \mathbf{f}_{\mathbf{Z}})}_{\text{update}}. \quad (9)$$

$$\approx \sum_{i=1}^S \mathbf{w}_i \phi_i(\mathbf{x}) + \sum_{j=1}^M \nu_j K(\mathbf{x}, \mathbf{z}_j), \quad (10)$$

where we use S Fourier bases $\phi_i(\cdot)$ with $\mathbf{w}_i \sim \mathcal{N}(\mathbf{0}, I)$ (Rahimi and Recht, 2007; Brault et al., 2016) to represent the stationary prior, and function basis $K(\cdot, \mathbf{z}_j)$ for the posterior update with $\nu = K(\mathbf{Z}, \mathbf{Z})^{-1}(\mathbf{U} - \Phi \mathbf{W})$, $\Phi = \phi(\mathbf{Z}) \in \mathbb{R}^{M \times S}$, $\mathbf{W} \in \mathbb{R}^{S \times D}$. By combining these two steps, we can accurately evaluate functions from the posterior (7) in linear time at arbitrary locations. We refer the reader to the supplementary section for more details.

3.4 Augmenting the ODE model with shooting system

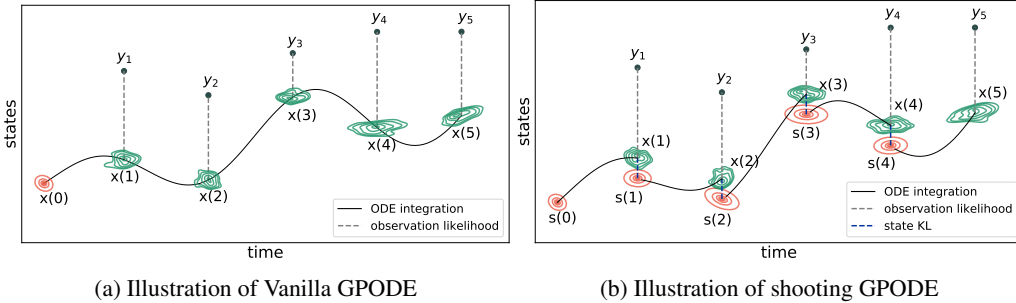


Figure 2: Illustrations of shooting augmentation: (a) in the vanilla GPODE formulation, the initial state distribution \mathbf{x}_0 is integrated forward in time to match all the observations $\{\mathbf{y}_1, \dots, \mathbf{y}_N\}$ forming a full trajectory. (b) The shooting version splits the full trajectory into multiple subintervals. Every subinterval i starts with an approximated state distribution \mathbf{s}_i , which is integrated forward to match the next observation \mathbf{y}_{i+1} . In addition, the state evolution from the previous shooting variable \mathbf{s}_{i-1} is matched to the variational approximation for the current state \mathbf{s}_i .

A key bottleneck in ODE modeling is the poor gradient descent performance over long integration times $\mathbf{x}_{0:T}$, which can exhibit vanishing or exploding gradients (Haber and Ruthotto, 2017; Choromanski et al., 2020; Kim et al., 2021). Earlier approaches tackled this issue mainly with more accurate numerical solvers (Zhuang et al., 2020, 2021). The nonlinearity of the integration map $\mathbf{x}_0 \mapsto \mathbf{x}_t$ motivates us to instead propose to segment the full integration $\mathbf{x}_{0:T}$ into short segments, which are easier to optimize and can be trivially parallelized (Aydogmus and Tor, 2021). This is denoted as the ‘multiple shooting’ method in optimal control literature (Osborne, 1969; Bock and Plitt, 1984);

see [Diehl and Gros \(2017\)](#) and [Peifer and Timmer \(2007\)](#) for reviews. We introduce a probabilistic shooting method for the Gaussian process posterior inference of ODEs.

We begin by augmenting the ODE with shooting states $\mathbf{s}(t)$ and shooting variables $\mathbf{S} = \{\mathbf{s}_i\}_{i=1}^{N-1}$,

$$\mathbf{x}(t) = \mathbf{s}_{i-1} + \int_{t_{i-1}}^{t_i} \mathbf{f}(\mathbf{x}(\tau))d\tau, \quad t \in [t_{i-1}, t_i] \quad (11)$$

$$\mathbf{s}(t_i) = \mathbf{s}_{i-1} + \int_{t_{i-1}}^{t_i} \mathbf{f}(\mathbf{s}(\tau))d\tau, \quad (12)$$

where we segment the state function $\mathbf{x}(t)$ into N pieces of length $t_i - t_{i-1}$ that branch from the shooting states \mathbf{s}_{i-1} , while both models follow the same differential \mathbf{f} . The augmented system is equivalent to the original ODE system if we constrain $\mathbf{s}_i = \mathbf{x}(t_i)$.

The joint probability of the augmented model is

$$p(\mathbf{Y}, \mathbf{X}, \mathbf{S}, \mathbf{f}) = \prod_{i=1}^N \underbrace{p(\mathbf{y}_i|\mathbf{x}_i)}_{\text{likelihood}} \underbrace{p(\mathbf{x}_i|\mathbf{s}_{i-1}, \mathbf{f})}_{\text{state transition}} \prod_{i=1}^{N-1} \underbrace{p(\mathbf{s}_i|\mathbf{s}_{i-1}, \mathbf{f})}_{\text{latent transition}} \underbrace{p(\mathbf{s}_0)}_{\text{state prior}} \underbrace{p(\mathbf{f})}_{\text{GP prior}}, \quad (13)$$

where now each state \mathbf{x}_i is decoupled from earlier states. This allows solving each segment in parallel. See supplementary section for a plate diagram and detailed derivation of the approach.

3.5 Inference for the augmented model

To infer the augmented posterior $p(\mathbf{f}, \mathbf{S}|\mathbf{Y})$ we introduce variational shooting approximation $q(\mathbf{S}) = q(\mathbf{s}_0) \cdots q(\mathbf{s}_{N-1})$, where each distribution $q(\mathbf{s}_i) \sim \mathcal{N}(\mathbf{a}_i, \Sigma_i)$ is a Gaussian. This results in the full variational posterior

$$q(\mathbf{S}, \mathbf{f}, \mathbf{U}) = \prod_{i=0}^{N-1} q(\mathbf{s}_i)p(\mathbf{f}|\mathbf{U})q(\mathbf{U}), \quad (14)$$

with the corresponding shooting ELBO

$$\begin{aligned} \mathcal{L}_{\text{shooting}} = & \sum_{i=1}^N \overbrace{\mathbb{E}_{q_{\rightarrow}(\mathbf{x}_i)} \log p(\mathbf{y}_i|\mathbf{x}_i)}^{\text{variational likelihood}} - \sum_{i=1}^{N-1} \overbrace{\text{KL}[q(\mathbf{s}_i) || q_{\rightarrow}(\mathbf{s}_i)]}^{\text{ODE matching}} \\ & - \text{KL}[q(\mathbf{s}_0)||p(\mathbf{s}_0)] - \text{KL}[q(\mathbf{U})||p(\mathbf{U})]. \end{aligned} \quad (15)$$

The key term in the ELBO is the ODE matching term, where the Gaussian pointwise approximation $q(\mathbf{s}_i)$ is matched via KL with the non-linear ODE evolution $q_{\rightarrow}(\mathbf{s}_i) = \mathbb{E}_{\mathbf{f}} q_{\rightarrow}(\mathbf{s}_i|\mathbf{f})$ from the previous shooting state \mathbf{s}_{i-1} (See Figure 2). This distribution is a continuous-time normalizing flow ([Chen et al., 2018](#))

$$\log q_{\rightarrow}(\mathbf{s}_i|\mathbf{f}) = \log q_{i-1}(\tilde{\mathbf{s}}_{i-1}) + \int_{t_i}^{t_{i-1}} \text{tr} \left(\frac{\partial \mathbf{f}(\mathbf{s}(t))}{\partial \mathbf{s}(t)} \right) dt, \quad (16)$$

$$\tilde{\mathbf{s}}_{i-1} = \mathbf{s}_i + \int_{t_i}^{t_{i-1}} \mathbf{f}(\mathbf{s}(\tau))d\tau, \quad (17)$$

where the trajectory follows the ODE (12). The term $q_{\rightarrow}(\mathbf{x}_i)$ in (15) is defined similarly. We refer the reader to the supplementary material for detailed derivations.

4 Experiments

We validate the proposed method on Van der Pol (VDP) and FitzHugh–Nagumo (FHN) systems and also on the task of learning human motion dynamics (MoCap). We use 16 inducing points in VDP and FHN experiments and 100 inducing points for the MoCap experiments. We consistently use squared exponential kernel with ARD and optimize kernel lengthscales, signal variance, noise variance, and inducing locations as hyperparameters. For the shooting version of GPODE, we found

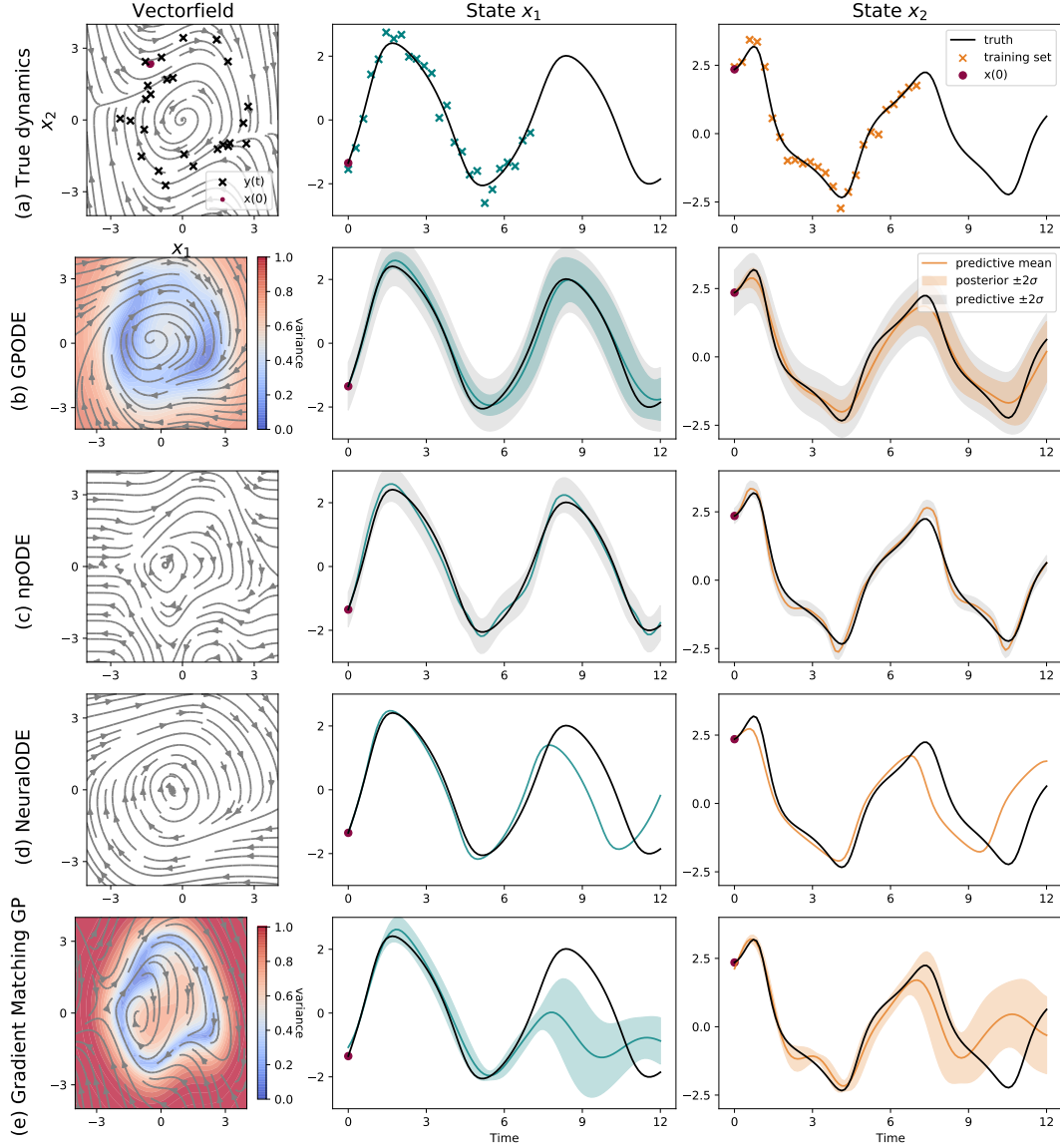


Figure 3: Learning the 2D Van der Pol dynamics (a) with alternative methods (b-e). Column 1 shows the vector fields while columns 2 and 3 show the state trajectories $x_1(t)$ and $x_2(t)$. GPODE learns the posterior accurately.

the inference of kernel signal variance to be problematic. We identified a constant scaling factor of 0.1 on the inducing KL term in equation 15 to fix this issue, inspired by VAE balancing factors (Alemi et al., 2018).

We use the implicit dopri15 solver with tolerance parameters $\text{rtol} = 1e^{-5}$ and $\text{atol} = 1e^{-5}$, and use the adjoint method for computing loss gradients with `torchdiffeq`² package (Chen et al., 2018). We repeat all the experiments 5 times with random initialization and report means and standard errors.

4.1 Learning Van der Pol dynamics

We first illustrate the effectiveness of the proposed method by inferring the vector field posterior on a two-dimensional VDP (see Figure 3),

$$\dot{x}_1 = x_2, \dot{x}_2 = -x_1 + 0.5x_2(1 - x_1^2), \quad x_1(0) = -1.5, x_2(0) = 2.5. \quad (18)$$

²<https://github.com/rtqichen/torchdiffeq>

	Task 1: Forecasting		Task 2: Varying x_0	
	MNLL (\downarrow)	MSE (\downarrow)	MNLL (\downarrow)	MSE (\downarrow)
GP gradient matching	1.47 ± 0.02	1.27 ± 0.01	-	-
NeuralODE	-	2.45 ± 0.18	-	0.11 ± 0.01
npODE	7.42 ± 1.88	0.29 ± 0.06	9.85 ± 1.63	0.53 ± 0.07
GPODE	0.60 ± 0.03	0.13 ± 0.01	0.35 ± 0.02	0.10 ± 0.01

Table 3: VDP system learning performance on forecasting (task 1) and varying initial state tasks (task 2). We report mean \pm standard error over 5 runs from different random initializations, best values bolded. (\uparrow): higher is better, (\downarrow) lower is better

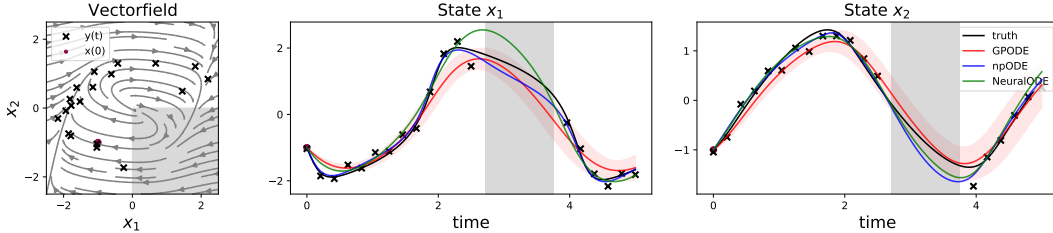


Figure 4: Learning FHN with gaps in data (gray region). The GPODE results in a useful posterior under data scarcity, while both NeuralODE and npODE result in some biases.

We simulate a trajectory of 50 regularly-sampled time points inside $t \in [0, 7]$, and add Gaussian noise with $\sigma^2 = 0.05$ to generate the training data. We explore two task scenarios: (1) forecasting the system dynamics between $t \in [7, 14]$, (2) forecasting the system from new initial states. In task 2, we generate new initial states by taking 100 samples from a Gaussian $\mathcal{N}(y_0, 0.04^2 I)$. We compare our GPODE model with npODE (Heinonen et al., 2018), NeuralODE (Chen et al., 2018), and gradient matched GPs (Ridderbusch et al., 2020).

Figure 3(b) shows that GPODE learns a vector field posterior, whose posterior mean closely matches the ground truth with low variance (blue regions) near the observed data. The posterior reduces back to the prior away from data (orange regions), indicating a good uncertainty characterization. The npODE seems to overfit, while the gradient matching GP cannot fit the model adequately. NeuralODE learns an appropriate vector field, but its long-term forecasting is biased. The NeuralODE and npODE models do not represent uncertainty, while the gradient matching GP posterior is poorly fit. A quantitative evaluation of the model fits in Table 3 indicate superior performance of GPODE.

4.2 Learning with missing observations

We illustrate the usefulness of learning Bayesian ODE posteriors under missing data with the FHN oscillator

$$\begin{aligned} \dot{x}_1 &= 3(x_1 - x_1^3/3 + x_2), \\ \dot{x}_2 &= (0.2 - 3x_1 - 0.2x_2)/3. \end{aligned} \quad (19)$$

	MNLL (\downarrow)	MSE (\downarrow)
NeuralODE	-	0.18 ± 0.00
npODE	6.49 ± 1.49	0.08 ± 0.01
GPODE	0.09 ± 0.05	0.07 ± 0.02

Table 2: Missing data results on the FHN system.

We generate a training sequence by simulating 25 regularly-sampled time points from $t \in [0, 5.0]$ with added Gaussian noise with $\sigma^2 = 0.025$. We remove all observations at quadrant $x_1 > 0, x_2 < 0$ and evaluate model accuracy in this region. Figure 4 shows that all models adequately learn smooth forecasts of missing states. The point estimates of npODE and NeuralODE have biases, while the GPODE posterior captures the uncertainty well (See Table 2).

4.3 Learning long trajectories with the shooting formulation

We demonstrate the necessity of the shooting formulation for working with long training trajectories. We use the VDP system with four observations per unit of time for $T = (25, 40, 55)$ corresponding to $N = (100, 160, 220)$ observed states. We also vary the observation variance as $\sigma^2 = (0.01, 0.05, 0.1)$. We test the model for forecasting additional 50 time points.

Figure 6 demonstrates that vanilla-GPODE and neuralODE fail to fit the data with long sequences on all noise levels. In contrast, inference for the shooting model is successful in all settings. The npODE is remarkably robust to long trajectories. All methods use high-performance gradient matching initialization for a realistic study (see supplementary)

Figure 5 shows a runtime trace comparison between vanilla GPODE and the shooting variant in wall-clock time for a fixed budget of 2000 optimization steps on VDP system with $N = 100$, $T = 25$ and $\sigma^2 = 0.01$. The shooting model converges approximately 10 times faster. The speedup stems from the parallelization of the shooting ODE solver since the shooting method splits the full IVP problem into numerous short and less non-linear IVPs. In addition, the shooting method relaxes the inference problem with its auxiliary augmentation. This experiment was conducted on a system with Nvidia GeForce GTX 1660S GPU.

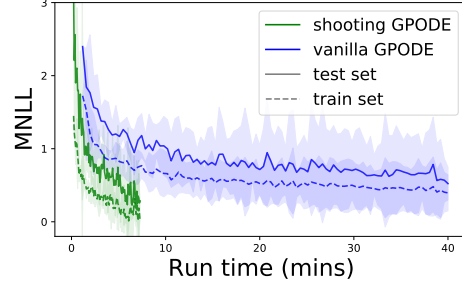


Figure 5: Optimization efficiency with shooting formulation

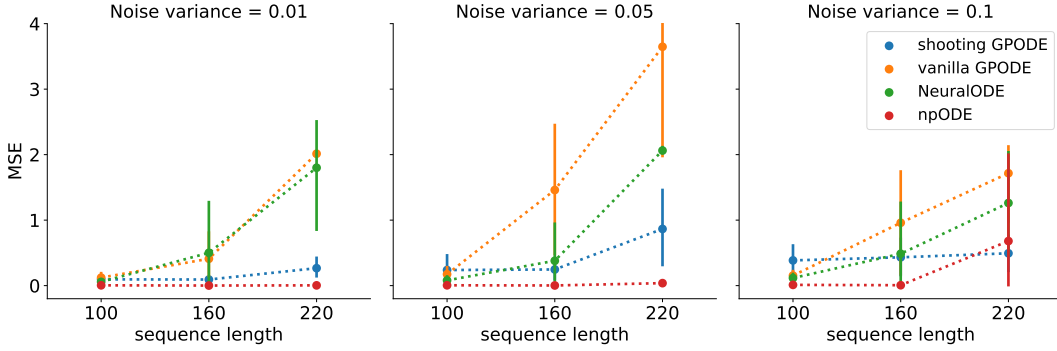


Figure 6: Varying sequence length and observation noise: shooting formulation makes GPODE feasible for long sequences, outperforming the non-shooting version and NeuralODE. The optimization for npODE is surprisingly good here. We report the results for different levels of observation noise on the VDP system.

4.4 Learning human motion dynamics

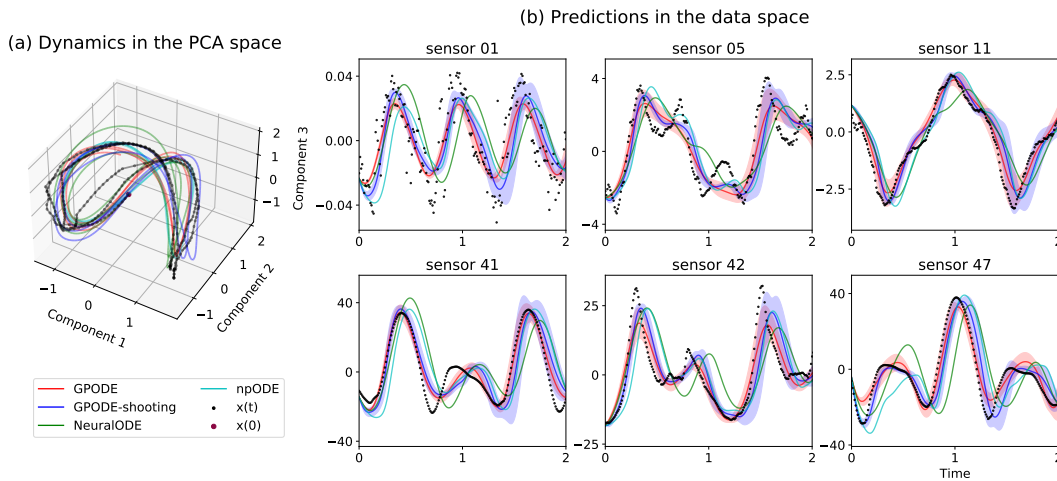


Figure 7: Learning the walking dynamics of subject 39: The true dynamics and predicted dynamics (mean) for the first three components in PCA space are shown in (a). Corresponding trajectories in the observation space for 6 different sensors are shown in (b) (We do not plot the observation noise variance for GPODE and npODE variants)

We learn the dynamics of human motion from noisy experimental data from CMU MoCap database for three subjects 09, 35 and 39. The dataset consists of 50 sensor readings from different parts of the body while walking or running. We follow the preprocessing of Wang et al. (2008) and center the data. The dataset was further split into train, test, and validation sequences (see the supplementary section for details on data size). We observed that both the NeuralODE and npODE models suffer from over-fitting, and we remedy this by applying early stopping by monitoring the validation loss during optimization.

We project the original 50-dimensional data into a 5-dimensional latent space using PCA and learn the dynamics in the latent space (Heinonen et al., 2018). To compute the data likelihood, we project the latent dynamics back to the original data space by inverting the PCA. We divide the experiment into sub-tasks MoCap-short and MoCap-long, based on the length of the sequence considered for model training (see the supplementary section for more details on the experimental setup). We measure the predictive performance on unseen test sequences in both tasks.

MNLL (\downarrow)	Subject 09		Subject 35		Subject 39	
	short	long	short	long	short	long
npODE	2.20 \pm 0.05	1.75 \pm 0.10	1.72 \pm 0.04	1.55 \pm 0.06	2.05 \pm 0.07	1.66 \pm 0.06
GPODE-vanilla	1.83 \pm 0.13	1.38 \pm 0.02	1.09 \pm 0.07	1.38 \pm 0.07	1.36 \pm 0.03	1.31 \pm 0.01
GPODE-shooting	1.66 \pm 0.03	1.79 \pm 0.00	1.53 \pm 0.00	1.59 \pm 0.01	1.85 \pm 0.01	1.82 \pm 0.00

Table 4: Test MNLL for dynamics prediction task on CMU MoCap dataset.

MSE (\downarrow)	Subject 09		Subject 35		Subject 39	
	short	long	short	long	short	long
NeuralODE	35.6 \pm 5.6	21.0 \pm 2.8	26.4 \pm 0.6	21.4 \pm 0.1	111.7 \pm 15.2	41.3 \pm 3.8
npODE	84.5 \pm 27.5	23.7 \pm 6.5	29.1 \pm 3.4	16.1 \pm 3.7	90.5 \pm 21.6	41.0 \pm 5.3
GPODE-vanilla	24.1 \pm 4.0	11.0 \pm 0.4	14.8 \pm 2.8	15.9 \pm 1.1	29.9 \pm 3.9	22.2 \pm 1.4
GPODE-shooting	22.1 \pm 3.1	10.2 \pm 0.5	11.6 \pm 0.6	22.1 \pm 0.7	28.1 \pm 4.2	21.1 \pm 0.7

Table 5: Test MSE for dynamics prediction task on CMU MoCap dataset.

Tables 4 and 5 indicate that GPODE outperforms the state-of-the-art npODE and NeuralODE methods. The slower vanilla-GPODE variant has superior MNLL performance, while the shooting-GPODE has better MSE metrics. This is natural due to the shooting method being more approximative but more efficient due to its augmentation. Figure 7 visualises the predicted dynamics for a test sequence. The GPODE variants have reasonable posterior uncertainties, while neuralODE and npODE tend to be overconfident and make more mistakes (see Figure 7 (b) sensors 01, 41 and 47). We note that some variations in the data space cannot be accurately estimated due to the low-dimensional PCA projection.

5 Conclusion and discussion

We proposed a novel model for Bayesian inference of ODEs using Gaussian processes. With this approach, one can model unknown ODE systems directly from the observational data and learn posteriors of the continuous-time vector fields. In contrast, earlier works produce point estimate solutions. We believe this to be a significant addition to the data-descriptive ODE modeling methods, especially for applications where uncertainty quantification is critical. In addition, many conventional machine learning algorithms have been interpreted and modeled as continuous-time dynamical systems, with applications to variational inference and density estimation (Grathwohl et al., 2019). Free-form ODE models can also be considered for applications like monotonic regression and probabilistic alignment (Ustyuzhaninov et al., 2020). The proposed model can be used as a plug-in extension in these applications.

We also highlighted a problem of learning black-box ODE models on long trajectories and proposed a probabilistic shooting framework enabling efficient inference on such tasks. This framework can be applied to other existing approaches, including NeuralODEs. One could also consider improving

the inference for shooting approximations similar to the works (Ialongo et al., 2019) from discrete domains.

References

- Tarmo Äijö and Harri Lähdesmäki. Learning gene regulatory networks from gene expression measurements using non-parametric molecular kinetics. *Bioinformatics*, 25(22):2937–2944, 2009.
- Alexander Alemi, Ben Poole, Ian Fischer, Joshua Dillon, Rif Saurous, and Kevin Murphy. Fixing a broken ELBO. In *International Conference on Machine Learning*, pages 159–168, 2018.
- Mauricio Alvarez, Lorenzo Rosasco, and Neil Lawrence. Kernels for vector-valued functions: A review. *Foundations and Trends in Machine Learning*, 4:195–266, 2012.
- Ozgur Aydogmus and Ali Tor. A modified multiple shooting algorithm for parameter estimation in odes using adjoint sensitivity analysis. *Applied Mathematics and Computation*, 390:125644, 2021.
- Mohamed Bhouri and Paris Perdikaris. Gaussian processes meet NeuralODEs: A Bayesian framework for learning the dynamics of partially observed systems from scarce and noisy data. *arXiv*, 2021.
- David Blei, Alp Kucukelbir, and Jon D McAuliffe. Variational inference: A review for statisticians. *Journal of the American statistical Association*, 112(518):859–877, 2017.
- Hans Bock and Karl Plitt. A multiple shooting algorithm for direct solution of optimal control problems. In *IFAC World Congress*, pages 242–247, 1984.
- Romain Brault, Markus Heinonen, and Florence Buc. Random Fourier features for operator-valued kernels. In *Asian Conference on Machine Learning*, pages 110–125, 2016.
- Steven Brunton, Joshua Proctor, and Nathan Kutz. Discovering governing equations from data by sparse identification of nonlinear dynamical systems. *PNAS*, 113(15):3932–3937, 2016.
- John Butcher and Nicolette Goodwin. *Numerical methods for ordinary differential equations*. Wiley Online Library, 2nd edition, 2008.
- Ben Calderhead, Mark Girolami, and Neil Lawrence. Accelerating Bayesian inference over nonlinear differential equations with Gaussian processes. In *Advances in Neural Information Processing Systems*, 2008.
- Tian Qi Chen, Yulia Rubanova, Jesse Bettencourt, and David Duvenaud. Neural ordinary differential equations. In *Advances in Neural Information Processing Systems*, pages 6571–6583, 2018.
- Krzysztof Choromanski, Jared Davis, Valerii Likhoshesterov, Xingyou Song, Jean-Jacques Slotine, Jacob Varley, Honglak Lee, Adrian Weller, and Vikas Sindhwani. An Ode to an ODE. In *Advances in Neural Information Processing Systems*, volume 33, 2020.
- Moritz Diehl and Sebastian Gros. *Numerical Optimal Control*. University of Freiburg, 2017.
- Andreas Doerr, Christian Daniel, Martin Schiegg, Nguyen-Tuong Duy, Stefan Schaal, Marc Toussaint, and Trimpe Sebastian. Probabilistic recurrent state-space models. In *International Conference on Machine Learning*, pages 1280–1289, 2018.
- Frank Dondelinger, Dirk Husmeier, Simon Rogers, and Maurizio Filippone. ODE parameter inference using adaptive gradient matching with Gaussian processes. In *Artificial Intelligence and Statistics*, pages 216–228, 2013.
- Stefanos Eleftheriadis, Tom Nicholson, Marc Peter Deisenroth, and James Hensman. Identification of Gaussian process state space models. In *Advances in Neural Information Processing Systems*, pages 5309–5319, 2017.
- Roger Frigola, Yutian Chen, and Carl Rasmussen. Variational Gaussian process state-space models. In *Advances in Neural Information Processing Systems*, 2014.
- Mark Girolami. Bayesian inference for differential equations. *Theoretical Computer Science*, 408: 4–16, 2008.

- Will Grathwohl, Ricky T. Q. Chen, Jesse Bettencourt, Ilya Sutskever, and David Duvenaud. FFJORD: Free-form continuous dynamics for scalable reversible generative models. In *ICLR*, 2019.
- Eldad Haber and Lars Ruthotto. Stable architectures for deep neural networks. *Inverse Problems*, 34: 014004, 2017.
- Markus Heinonen and Florence d’Alché-Buc. Learning nonparametric differential equations with operator-valued kernels and gradient matching. Technical report, Universite d’Evry, 2014.
- Markus Heinonen, Cagatay Yildiz, Henrik Mannerström, Jukka Intosalmi, and Harri Lähdesmäki. Learning unknown ODE models with Gaussian processes. In *International Conference on Machine Learning*, pages 1959–1968, 2018.
- James Henderson and George Michailidis. Network reconstruction using nonparametric additive ODE models. *PLOS ONE*, 9(4):e94003, 2014.
- James Hensman, Nicolò Fusi, and Neil Lawrence. Gaussian processes for big data. In *Uncertainty in Artificial Intelligence*, pages 282–290, 2013.
- Morris Hirsch, Stephen Smale, and Robert Devaney. *Differential equations, dynamical systems, and an introduction to chaos*. Academic press, 2012.
- Alessandro Davide Ialongo, Mark Van Der Wilk, James Hensman, and Carl Edward Rasmussen. Overcoming mean-field approximations in recurrent gaussian process models. In *International Conference on Machine Learning*, pages 2931–2940, 2019.
- Suyong Kim, Weiqi Ji, Sili Deng, and Christopher Rackauckas. Stiff neural ordinary differential equations. *arXiv:2103.15341*, 2021.
- Diederik P Kingma and Jimmy Lei Ba. Adam: A method for stochastic optimization. In *Proceedings of 3rd International Conference on Learning Representations*, 2014.
- Petar Kokotovic and James Heller. Direct and adjoint sensitivity equations for parameter optimization. *IEEE Transactions on Automatic Control*, 12(5):609–610, 1967.
- Ernst Lindelöf. Sur l’application de la méthode des approximations successives aux équations différentielles ordinaires du premier ordre. *Comptes rendus hebdomadaires des séances de l’Académie des sciences*, 116:454–457, 1894.
- Benn Macdonald, Catherine Higham, and Dirk Husmeier. Controversy in mechanistic modelling with Gaussian processes. In *International Conference on Machine Learning*, pages 1539–1547, 2015.
- Michael Osborne. On shooting methods for boundary value problems. *Journal of Mathematical Analysis and Applications*, 27:417–433, 1969.
- Martin Peifer and Jens Timmer. Parameter estimation in ordinary differential equations using the method of multiple shooting. *IET Systems Biology*, 1:78–88, 2007.
- Lev Pontryagin, Evgenii Mishchenko, Vladimir Boltyanskii, and Revas Gamkrelidze. *The mathematical theory of optimal processes*. Interscience Publishers, 1962. Translation KN Trirogoff.
- Christopher Rackauckas and Qing Nie. Differentialequations.jl – a performant and feature-rich ecosystem for solving differential equations in Julia. *Journal of Open Research Software*, 5(1), 2017.
- Ali Rahimi and Benjamin Recht. Random features for large-scale kernel machines. In *Advances in Neural Information Processing Systems*, pages 1177–1184, 2007.
- Jim Ramsay, Giles Hooker, David Campbell, and Jiguo Cao. Parameter estimation for differential equations: A generalized smoothing approach. *Journal of the Royal Statistical Society: Series B*, 69(5):741–796, 2007.
- Carl Rasmussen and Christopher Williams. *Gaussian processes for machine learning*. The MIT Press, 2006.

- Steffen Ridderbusch, Christian Offen, Sina Ober-Blöbaum, and Paul Goulart. Learning ODE models with qualitative structure using Gaussian processes. *arXiv:2011.05364*, 2020.
- Simone Rossi, Markus Heinonen, Edwin Bonilla, Zheyang Shen, and Maurizio Filippone. Sparse Gaussian processes revisited: Bayesian approaches to inducing-variable approximations. In *Artificial Intelligence and Statistics*, pages 1837–1845, 2021.
- Yulia Rubanova, Ricky T. Q. Chen, and David Duvenaud. Latent ODEs for irregularly-sampled time series. In *Advances in Neural Information Processing Systems*, 2019.
- Development Team Stan. Stan modeling language users guide and reference manual, mc-stan.org. 2021.
- Michalis Titsias. Variational learning of inducing variables in sparse Gaussian processes. In *Artificial Intelligence and Statistics*, pages 567–574, 2009.
- Ryan Turner, Marc Deisenroth, and Carl Rasmussen. State-space inference and learning with Gaussian processes. In *Artificial Intelligence and Statistics*, pages 868–875, 2010.
- Ivan Ustyuzhaninov, Ieva Kazlauskaitė, Carl Henrik Ek, and Neill Campbell. Monotonic Gaussian process flows. In *Artificial Intelligence and Statistics*, volume 108, pages 3057–3067, 2020.
- James Varah. A spline least squares method for numerical parameter estimation in differential equations. *SIAM Journal on Scientific and Statistical Computing*, 3(1):28–46, 1982.
- Jack Wang, Aaron Hertzmann, and David Fleet. Gaussian process dynamical models. In *Advances in Neural Information Processing Systems*, 2005.
- Jack Wang, David Fleet, and Aaron Hertzmann. Gaussian process dynamical models for human motion. *IEEE Transactions on Pattern Analysis and Machine Intelligence*, 30(2):283–298, 2008.
- Philippe Wenk, Gabriele Abbati, Michael Osborne, Bernhard Schölkopf, Andreas Krause, and Stefan Bauer. ODIN: ODE-informed regression for parameter and state inference in time-continuous dynamical systems. In *AAAI Conference on Artificial Intelligence*, volume 34, pages 6364–6371, 2020.
- James Wilson, Viacheslav Borovitskiy, Alexander Terenin, Peter Mostowsky, and Marc Deisenroth. Efficiently sampling functions from Gaussian process posteriors. In *International Conference on Machine Learning*, pages 10292–10302, 2020.
- Cagatay Yildiz, Markus Heinonen, and Harri Lähdesmäki. ODE2VAE: Deep generative second order ODEs with Bayesian neural networks. In *Advances in Neural Information Processing Systems*, pages 13412–13421, 2019.
- Juntang Zhuang, Nicha Dvornek, Xiaoxiao Li, Sekhar Tatikonda, Xenophon Papademetris, and James Duncan. Adaptive checkpoint adjoint method for gradient estimation in neural ODE. In *International Conference on Machine Learning*, pages 11639–11649, 2020.
- Juntang Zhuang, Nicha Dvornek, Sekhar Tatikonda, and James Duncan. MALI: A memory efficient and reverse accurate integrator for neural ODEs. In *ICLR*, 2021.
- Tarmo Äijö, Kirsi Granberg, and Harri Lähdesmäki. Sorad: A systems biology approach to predict and modulate dynamic signaling pathway response from phosphoproteome time-course measurements. *Bioinformatics*, 29:1283–1291, 2013.

Supplementary material for Bayesian inference of ODEs with Gaussian processes

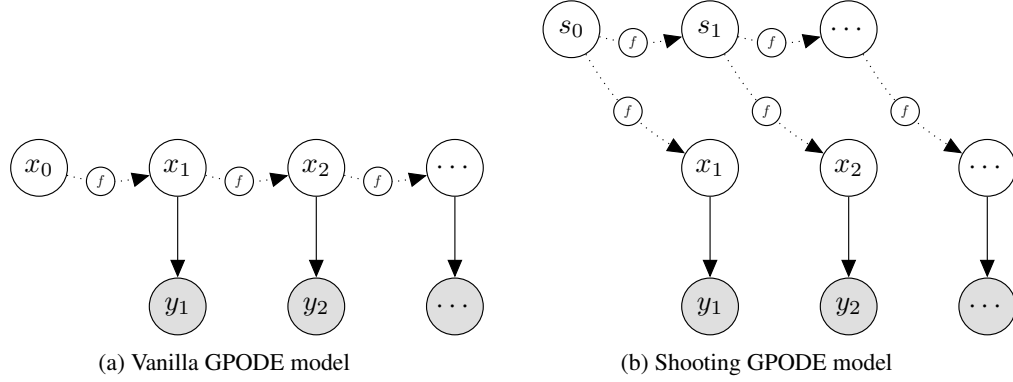


Figure 1: Plate diagrams: in the vanilla GPODE formulation (a), the initial state distribution \mathbf{x}_0 is integrated forward in time to match all the observations $\{\mathbf{y}_1, \mathbf{y}_2, \dots, \mathbf{y}_N\}$ forming a full trajectory. The shooting version (b) splits the full trajectory into multiple subintervals. Every subinterval i starts with an approximated state distribution s_i , which is integrated forward to match the next observation \mathbf{y}_{i+1} . In addition, the state evolution from the previous shooting variable is matched to the variational shooting approximation at the current state.

Inference for the vanilla GPODE model

The model. We consider the problem of inferring an ODE system

$$\mathbf{y}(t) = \mathbf{x}(t) + \epsilon \quad (1)$$

$$\mathbf{x}(t) = \mathbf{x}_0 + \int_0^t \mathbf{f}(\mathbf{x}(\tau)) d\tau \quad (2)$$

$$(3)$$

from some noisy observations $\mathbf{y}(t)$ of the true system state $\mathbf{x}(t) \in \mathbb{R}^D$, whose evolution over time $t \in \mathbb{R}_+$ follows a differential equation vector field

$$\dot{\mathbf{x}}(t) = \frac{d\mathbf{x}(t)}{dt} := \mathbf{f}(\mathbf{x}(t)), \quad \mathbf{f} : \mathbb{R}^D \mapsto \mathbb{R}^D \quad (4)$$

starting from initial state $\mathbf{x}_0 \in \mathbb{R}^D$. Our goal is to learn the underlying ODE vector field \mathbf{f} .

We propose a Gaussian process prior for the differential function

$$\mathbf{f}(\mathbf{x}) \sim \mathcal{GP}(\mathbf{0}, k(\mathbf{x}, \mathbf{x}')) \quad (5)$$

$$p(\mathbf{f}) = \mathcal{N}(\mathbf{f} | \mathbf{0}, \mathbf{K}_{\mathbf{xx}}). \quad (6)$$

Following [Titsias \(2009\)](#) for sparse inference of GPs using inducing variables, we augment the full model with inducing values $\mathbf{U} = (\mathbf{u}_1, \dots, \mathbf{u}_M)^T \in \mathbb{R}^{M \times D}$ and inducing locations $\mathbf{Z} = (\mathbf{z}_1, \dots, \mathbf{z}_M)^T \in \mathbb{R}^{M \times D}$, which results in a low-rank GP

$$p(\mathbf{U}) = \mathcal{N}(\mathbf{U} | \mathbf{0}, \mathbf{K}_{\mathbf{zz}}) \quad (7)$$

$$p(\mathbf{f} | \mathbf{U}) = \mathcal{N}(\mathbf{f} | \mathbf{A} \text{vec}(\mathbf{U}), \mathbf{K}_{\mathbf{xx}} - \mathbf{A} \mathbf{K}_{\mathbf{zz}} \mathbf{A}^T), \quad (8)$$

where $\mathbf{X} = (\mathbf{x}_1, \mathbf{x}_2, \dots, \mathbf{x}_{N'})^T \in \mathbb{R}^{N' \times D}$ collects all the intermediate state evaluations $\mathbf{x}(t_i)$ encountered along numerical approximation of the true continuous ODE integral (2), $\mathbf{f} = (\mathbf{f}(\mathbf{x}_1)^T, \dots, \mathbf{f}(\mathbf{x}_{N'})^T)^T \in \mathbb{R}^{N' \times D}$, $\mathbf{K}_{\mathbf{xx}}$ is a block-partitioned matrix of size $N'D \times N'D$ with $D \times D$ blocks, so that block $(\mathbf{K}_{\mathbf{xx}})_{i,j} = K(\mathbf{x}_i, \mathbf{x}_j)$, and $\mathbf{A} = \mathbf{K}_{\mathbf{xz}} \mathbf{K}_{\mathbf{zz}}^{-1}$.

The joint model. The joint probability of the model is

$$p(\mathbf{Y}, \mathbf{f}, \mathbf{U}, \mathbf{x}_0) = \prod_{i=1}^N p(\mathbf{y}_i | \mathbf{f}, \mathbf{x}_0) p(\mathbf{f} | \mathbf{U}) p(\mathbf{U}) p(\mathbf{x}_0) \quad (9)$$

$$= \prod_{i=1}^N \underbrace{p(\mathbf{y}_i | \mathbf{f}, \mathbf{x}_0)}_{\text{likelihood}} \underbrace{p(\mathbf{f}, \mathbf{U})}_{\text{GP prior}} \underbrace{p(\mathbf{x}_0)}_{\text{initial state prior}}, \quad (10)$$

where we assume a standard Gaussian prior $p(\mathbf{x}_0) = \mathcal{N}(\mathbf{0}, \mathbf{I})$ for the unknown initial state \mathbf{x}_0 .

Inference. Our primary goal is to learn the vector field \mathbf{f} by inferring the model posterior $p(\mathbf{f}, \mathbf{U}, \mathbf{x}_0 | \mathbf{y})$, which is intractable. We resort to stochastic variational inference [Hensman et al. \(2013\)](#), and introduce a factorized Gaussian posterior approximation for the inducing variables across state dimensions

$$q(\mathbf{U}) = \prod_{d=1}^D \mathcal{N}(\mathbf{u}_d | \mathbf{m}_d, \mathbf{Q}_d), \quad (11)$$

where, $\mathbf{u}_d \in \mathbb{R}^M$ and $\mathbf{m}_d \in \mathbb{R}^M$, $\mathbf{Q}_d \in \mathbb{R}^{M \times M}$ are the mean and covariance parameters of the variational Gaussian posterior approximation for the inducing variables. The Gaussian process posterior process with an inducing approximation can be written as

$$q(\mathbf{f}) = \int p(\mathbf{f} | \mathbf{U}) q(\mathbf{U}) d\mathbf{U} \quad (12)$$

$$= \int \mathcal{N}(\mathbf{f} | \mathbf{A} \text{vec}(\mathbf{U}), \mathbf{K}_{\mathbf{X}\mathbf{X}} - \mathbf{A} \mathbf{K}_{\mathbf{Z}\mathbf{Z}} \mathbf{A}^T) q(\mathbf{U}) d\mathbf{U}. \quad (13)$$

We also introduce posterior approximation for the initial state variable \mathbf{x}_0 ,

$$q(\mathbf{x}_0) = \mathcal{N}(\mathbf{x}_0 | \mathbf{m}_0, \mathbf{S}_0). \quad (14)$$

This results in a variational joint posterior approximation

$$q(\mathbf{f}, \mathbf{U}, \mathbf{x}_0) = q(\mathbf{f}, \mathbf{U}) q(\mathbf{x}_0) \quad (15)$$

$$= p(\mathbf{f} | \mathbf{U}) q(\mathbf{U}) q(\mathbf{x}_0), \quad (16)$$

ELBO. With the above model specification, under variational inference the posterior approximations, the evidence lower bound (ELBO) $\log p(\mathbf{Y}) \geq \mathcal{L}$ can be written as,

$$\mathcal{L} = \iiint q(\mathbf{f}, \mathbf{U}, \mathbf{x}_0) \log \frac{p(\mathbf{Y}, \mathbf{f}, \mathbf{U}, \mathbf{x}_0)}{q(\mathbf{f}, \mathbf{U}, \mathbf{x}_0)} d\mathbf{f} d\mathbf{U} d\mathbf{x}_0 \quad (17)$$

$$= \iiint q(\mathbf{f}, \mathbf{U}, \mathbf{x}_0) \log \prod_{i=1}^N \underbrace{p(\mathbf{y}_i | \mathbf{f}, \mathbf{x}_0)}_{\mathcal{L}_y} \underbrace{\frac{p(\mathbf{f} | \mathbf{U})}{p(\mathbf{f} | \mathbf{U})}}_{\mathcal{L}_u} \underbrace{\frac{p(\mathbf{U})}{q(\mathbf{U})} \frac{p(\mathbf{x}_0)}{q(\mathbf{x}_0)}}_{\mathcal{L}_{\mathbf{x}_0}} d\mathbf{f} d\mathbf{U} d\mathbf{x}_0. \quad (18)$$

hence the ELBO decomposes into three additive terms

$$\mathcal{L} = \mathcal{L}_y + \mathcal{L}_u + \mathcal{L}_{\mathbf{x}_0}, \quad (19)$$

where each term contains the (relevant parts of) expectation over $q(\mathbf{f}, \mathbf{U}, \mathbf{x}_0)$.

Likelihood term. The variational likelihood term \mathcal{L}_y is an expectation of the likelihood wrt the variationally marginalized vectorfield posterior $q(\mathbf{f})$, and the initial state distribution $q(\mathbf{x}_0)$,

$$\mathcal{L}_y = \iint q(\mathbf{f}, \mathbf{x}_0) \log p(\mathbf{y} | \mathbf{f}, \mathbf{x}_0) d\mathbf{f} d\mathbf{x}_0 \quad (20)$$

$$= \sum_{i=1}^N \mathbb{E}_{q(\mathbf{f}, \mathbf{x}_0)} \log p(\mathbf{y}_i | \mathbf{f}, \mathbf{x}_0). \quad (21)$$

This term computes the likelihood $p(\mathbf{y}_i|\mathbf{f}, \mathbf{x}_0) = p(\mathbf{y}_i|\mathbf{x}_i)$ over ODE state solutions $\mathbf{x}_i = \mathbf{x}_0 + \int_0^{t_i} \mathbf{f}(\mathbf{x}(\tau))d\tau$ for a single realization of vector field $\mathbf{f} \sim p(\mathbf{f})$ and the initial state $\mathbf{x}_0 \sim p(\mathbf{x}_0)$. Because of the non-linear integration $\mathbf{x}_0 \mapsto \mathbf{x}(t)$, we cannot solve this integral analytically. Instead we resort to Monte Carlo integration by sampling ODE trajectories over for different vector field realizations $\mathbf{f} \sim q(\mathbf{f})$ and initial states $\mathbf{x}_0 \sim q(\mathbf{x}_0)$. In practice this term can be approximated as

$$\mathcal{L}_y \approx \frac{1}{S} \sum_{s=1}^S \sum_{i=1}^N \log p(\mathbf{y}_i|\mathbf{f}^{(s)}, \mathbf{x}_0^{(s)}) \quad (22)$$

where we sum over S reparameterized samples $\mathbf{f}^{(s)} \sim q(\mathbf{f})$ and $\mathbf{x}_0^{(s)} \sim q(\mathbf{x}_0)$.

Inducing KL. This term corresponds to the KL divergence between variational posterior and the prior distribution of inducing values. This term can be derived analytically as the KL between multivariate Gaussians.

$$\mathcal{L}_u = \int q(\mathbf{U}) \log \frac{p(\mathbf{U})}{q(\mathbf{U})} d\mathbf{U} \quad (23)$$

$$= \sum_{d=1}^D \int q(\mathbf{u}_d) \log \frac{p(\mathbf{u}_d)}{q(\mathbf{u}_d)} d\mathbf{u} \quad (24)$$

$$= - \sum_{d=1}^D \text{KL}[q(\mathbf{u}_d)||p(\mathbf{u}_d)] \quad (25)$$

Initial state KL. This term corresponds to the KL divergence between variational posterior and the prior distribution of the initial state. With an assumption of Gaussian prior and variational posterior, this term can also be derived analytically,

$$\mathcal{L}_{\mathbf{x}_0} = \int q(\mathbf{x}_0) \log \frac{p(\mathbf{x}_0)}{q(\mathbf{x}_0)} d\mathbf{x}_0 \quad (26)$$

$$= - \text{KL}[q(\mathbf{x}_0)||p(\mathbf{x}_0)] \quad (27)$$

Complete ELBO. The full ELBO is then

$$\mathcal{L} = \sum_{i=1}^N \mathbb{E}_{q(\mathbf{f}, \mathbf{x}_0)} \log p(\mathbf{y}_i|\mathbf{f}, \mathbf{x}_0) - \text{KL}[q(\mathbf{U})||p(\mathbf{U})] - \text{KL}[q(\mathbf{x}_0)||p(\mathbf{x}_0)] \quad (28)$$

Decoupled sampling of GPODEs

In this section we provide details for simulating valid ODE trajectories from a GP vector field posterior of the form

$$q(\mathbf{u}) = \mathcal{N}(\mathbf{m}, \mathbf{Q}), \quad (29)$$

$$q(\mathbf{f}) = \int p(\mathbf{f}|\mathbf{u})q(\mathbf{u})d\mathbf{u} \quad (30)$$

$$= \int \mathcal{N}(\mathbf{f}|\mathbf{A}\mathbf{u}, \mathbf{K}_{\mathbf{X}\mathbf{X}} - \mathbf{A}\mathbf{K}_{\mathbf{Z}\mathbf{Z}}\mathbf{A}^T) q(\mathbf{u})d\mathbf{u}, \quad (31)$$

where $\mathbf{A} = \mathbf{K}_{\mathbf{X}\mathbf{Z}}\mathbf{K}_{\mathbf{Z}\mathbf{Z}}^{-1}$ and $\mathbf{m} \in \mathbb{R}^M$, $\mathbf{Q} \in \mathbb{R}^{M \times M}$ are the variational mean and covariance parameters of the Gaussian posterior approximation for inducing variables. For simplicity we have considered a scalar valued GP, but it straight forward to extend this approach to vector-valued GPs.

A sparse GP posterior of the form (31) can be decomposed into two parts using Matheron's rule (Corollary 2 Wilson et al. (2020)),

$$\underbrace{f(\mathbf{x})|\mathbf{u}}_{\text{posterior}} = \underbrace{f(\mathbf{x})}_{\text{prior}} + \underbrace{k(\mathbf{x}, \mathbf{Z})\mathbf{K}(\mathbf{Z}, \mathbf{Z})^{-1}(\mathbf{u} - \mathbf{f}_{\mathbf{Z}})}_{\text{update}}. \quad (32)$$

Wilson et al. (2020) propose a decoupled sampling from the posterior by using different bases for the prior and update terms. In particular, they propose Fourier basis functions for the prior term and canonical basis for the update term respectively

$$\underbrace{f(\mathbf{x})|\mathbf{u}}_{\text{posterior}} \approx \underbrace{\sum_{i=1}^S w_i \phi_i(\mathbf{x})}_{\text{prior}} + \underbrace{\sum_{j=1}^M \nu_j K(\mathbf{x}, \mathbf{z}_j)}_{\text{update}}, \quad (33)$$

where we use S Fourier bases $\phi_i(\cdot)$ with $w_i \sim \mathcal{N}(0, 1)$ (Rahimi and Recht, 2007; Brault et al., 2016) to represent the stationary prior, and function basis $K(\cdot, \mathbf{z}_j)$ for the posterior update with $\boldsymbol{\nu} = K(\mathbf{Z}, \mathbf{Z})^{-1}(\mathbf{u} - \Phi \mathbf{w})$, $\Phi = \phi(\mathbf{Z}) \in \mathbb{R}^{M \times S}$, $\mathbf{w} \in \mathbb{R}^S$. We can evaluate functions from the posterior (31) in linear time at arbitrary locations.

For the experimental results presented in the paper, we use squared exponential kernel for which we can compute the feature maps $\phi_i(\mathbf{x}) = \sqrt{\frac{\sigma_f^2}{S}} (\cos \mathbf{x}^T \boldsymbol{\omega}_i, \sin \mathbf{x}^T \boldsymbol{\omega}_i)$ where $\boldsymbol{\omega}_i$ is sampled proportional to the spectral density of the squared exponential kernel $\boldsymbol{\omega}_i \sim \mathcal{N}(\mathbf{0}, \Lambda^{-1})$, Λ is a diagonal matrix collecting lengthscale parameters of the kernel $\Lambda = \text{diag}(l_1^2, l_2^2, \dots, l_D^2)$ and σ_f^2 is the signal variance parameter. In the case of the squared exponential kernel, this results in $2S$ feature maps $\phi(\mathbf{x}) \in \mathbb{R}^{2S}$, for which we sample weights $\mathbf{w} \in \mathbb{R}^{2S}$ from the standard Normal $w_i \sim \mathcal{N}(0, 1)$. By fixing random samples of feature maps $\phi(\cdot)$, corresponding weights \mathbf{w} and inducing values \mathbf{u} for an ODE integration call, we can sample a unique ODE trajectory from a posterior vector field of the form (31).

Probabilistic shooting derivation for GPODE

The model. We consider the problem of inferring an ODE system

$$\mathbf{y}(t) = \mathbf{x}(t) + \boldsymbol{\epsilon} \quad (34)$$

$$\mathbf{x}(t) = \mathbf{x}_0 + \int_0^t \mathbf{f}(\mathbf{x}(\tau)) d\tau, \quad (35)$$

from some noisy observations $\mathbf{y}(t)$ of the true system state $\mathbf{x}(t) \in \mathbb{R}^D$, whose evolution over time $t \in \mathbb{R}_+$ follows a differential equation

$$\dot{\mathbf{x}}(t) = \frac{d\mathbf{x}(t)}{dt} := \mathbf{f}(\mathbf{x}(t)), \quad \mathbf{f} : \mathbb{R}^D \mapsto \mathbb{R}^D \quad (36)$$

starting from initial state $\mathbf{x}_0 \in \mathbb{R}^D$. Our goal is to learn the underlying ODE vector field \mathbf{f} .

Shooting augmentation. We propose an augmented ‘shooting’ ODE system

$$\mathbf{y}(t_i) = \mathbf{x}(t_i) + \boldsymbol{\epsilon} \quad (37)$$

$$\mathbf{x}(t_i) = \mathbf{s}_{i-1} + \int_{t_{i-1}}^{t_i} \mathbf{f}(\mathbf{x}(\tau)) d\tau \quad (38)$$

$$\mathbf{s}(t_i) = \mathbf{s}_{i-1} + \int_{t_{i-1}}^{t_i} \mathbf{f}(\mathbf{s}(\tau)) d\tau, \quad (39)$$

where we introduce an additional shooting ODE $\mathbf{s}(t)$ and segment the state function into N pieces that branch from the shooting model, while both models follow the same differential \mathbf{f} . The augmented system is equivalent to the original ODE system since the differential is shared.

Gaussian process ODE. We propose a Gaussian process prior for the differential function

$$\mathbf{f}(\mathbf{x}) \sim \mathcal{GP}(\mathbf{0}, k(\mathbf{x}, \mathbf{x}')) \quad (40)$$

$$p(\mathbf{f}) = \mathcal{N}(\mathbf{f} | \mathbf{0}, \mathbf{K}_{\mathbf{xx}}). \quad (41)$$

In addition, we augment the full model with inducing values $\mathbf{U} = (\mathbf{u}_1, \dots, \mathbf{u}_M)^T \in \mathbb{R}^{M \times D}$ and inducing locations $\mathbf{Z} = (\mathbf{z}_1, \dots, \mathbf{z}_M)^T \in \mathbb{R}^{M \times D}$, which results in a low-rank GP

$$p(\mathbf{U}) = \mathcal{N}(\mathbf{U} | \mathbf{0}, \mathbf{K}_{\mathbf{ZZ}}) \quad (42)$$

$$p(\mathbf{f} | \mathbf{U}) = \mathcal{N}(\mathbf{f} | \mathbf{A} \text{vec}(\mathbf{U}), \mathbf{K}_{\mathbf{xx}} - \mathbf{A} \mathbf{K}_{\mathbf{ZZ}} \mathbf{A}^T), \quad (43)$$

where $\mathbf{A} = \mathbf{K}_{\mathbf{xz}} \mathbf{K}_{\mathbf{zz}}^{-1}$.

The joint model. The joint probability of the model is

$$p(\mathbf{Y}, \mathbf{X}, \mathbf{S}, \mathbf{f}, \mathbf{U}) = \prod_{i=1}^N p(\mathbf{y}_i | \mathbf{x}_i) p(\mathbf{x}_i | \mathbf{s}_{i-1}, \mathbf{f}) \prod_{i=1}^{N-1} p(\mathbf{s}_i | \mathbf{s}_{i-1}, \mathbf{f}) p(\mathbf{s}_0) p(\mathbf{f} | \mathbf{U}) p(\mathbf{U}) \quad (44)$$

$$= \prod_{i=1}^N \underbrace{p(\mathbf{y}_i | \mathbf{x}_i)}_{\text{likelihood}} \underbrace{p(\mathbf{x}_i | \mathbf{s}_{i-1}, \mathbf{f})}_{\text{state ODE}} \prod_{i=1}^{N-1} \underbrace{p(\mathbf{s}_i | \mathbf{s}_{i-1}, \mathbf{f})}_{\text{shooting ODE}} \underbrace{p(\mathbf{s}_0)}_{\text{initial state}} \underbrace{p(\mathbf{f} | \mathbf{U}) p(\mathbf{U})}_{\text{GP prior}}, \quad (45)$$

where $\mathbf{X} = (\mathbf{x}_1, \mathbf{x}_2, \dots, \mathbf{x}_N)^T \in \mathbb{R}^{N \times D}$ collects all the state distributions $\mathbf{x}(t_i)$ at observation times and $\mathbf{S} = (\mathbf{s}_0, \mathbf{s}_1, \dots, \mathbf{s}_{N-1})^T \in \mathbb{R}^{N \times D}$ collects all shooting variables.

We also note that observations are at indices $1, \dots, N$, while the shooting variables are always one behind the observations at $0, \dots, N-1$ (see plate diagram 1 (b)).

Inference. Our primary goal is to learn the vector field \mathbf{f} by inferring the model posterior $p(\mathbf{X}, \mathbf{X}, \mathbf{f}, \mathbf{U} | \mathbf{Y})$, which is intractable. In a similar way to non-shooting GPODEs, we introduce a factorized Gaussian posterior approximation for the inducing variables across state dimensions

$$q(\mathbf{U}) = \prod_{d=1}^D \mathcal{N}(\mathbf{u}_d | \mathbf{m}_d, \mathbf{Q}_d), \quad (46)$$

where, $\mathbf{u}_d \in \mathbb{R}^M$ and $\mathbf{m}_d \in \mathbb{R}^M$, $\mathbf{Q}_d \in \mathbb{R}^{M \times M}$ are the mean and covariance parameters of the variational Gaussian posterior approximation for the inducing variables. The Gaussian process posterior process with an inducing approximation can be written as

$$q(\mathbf{f}) = \int p(\mathbf{f} | \mathbf{U}) q(\mathbf{U}) d\mathbf{U} \quad (47)$$

$$= \int \mathcal{N}(\mathbf{f} | \mathbf{A} \text{vec}(\mathbf{U}), \mathbf{K}_{\mathbf{X}\mathbf{X}} - \mathbf{A} \mathbf{K}_{\mathbf{Z}\mathbf{Z}} \mathbf{A}^T) q(\mathbf{U}) d\mathbf{U}. \quad (48)$$

Next, we introduce a factorized Gaussian posterior approximations for the shooting variables \mathbf{S} as well,

$$q(\mathbf{S}) = \prod_{i=0}^{N-1} q(\mathbf{s}_i) = \prod_{i=0}^{N-1} \mathcal{N}(\mathbf{s}_i | \mathbf{a}_i, \Sigma_i). \quad (49)$$

where, $\mathbf{a}_i \in \mathbb{R}^D$ and $\Sigma_i \in \mathbb{R}^{D \times D}$ are the mean and covariance parameters of the variational Gaussian posterior approximation for the shooting variables.

This results in a variational joint posterior approximation

$$q(\mathbf{X}, \mathbf{S}, \mathbf{f}, \mathbf{U}) = q(\mathbf{X}, \mathbf{S} | \mathbf{f}) q(\mathbf{f}, \mathbf{U}) \quad (50)$$

$$= \prod_{i=1}^N p(\mathbf{x}_i | \mathbf{s}_{i-1}, \mathbf{f}) \prod_{i=0}^{N-1} q(\mathbf{s}_i) p(\mathbf{f} | \mathbf{U}) q(\mathbf{U}). \quad (51)$$

ELBO. Under variational inference the posterior approximations q are optimised to match the true posterior in the KL sense,

$$\arg \min_q \text{KL} [q(\mathbf{X}, \mathbf{S}, \mathbf{f}, \mathbf{U}) || p(\mathbf{X}, \mathbf{S}, \mathbf{f}, \mathbf{U} | \mathbf{Y})]. \quad (52)$$

This is equivalent to maximizing the evidence lower bound (ELBO) $\log p(\mathbf{Y}) \geq \mathcal{L}$,

$$\mathcal{L} = \iiint q(\mathbf{X}, \mathbf{S}, \mathbf{f}, \mathbf{U}) \log \frac{p(\mathbf{Y}, \mathbf{X}, \mathbf{S}, \mathbf{f}, \mathbf{U})}{q(\mathbf{X}, \mathbf{S}, \mathbf{f}, \mathbf{U})} d\mathbf{X} d\mathbf{S} d\mathbf{f} d\mathbf{U} \quad (53)$$

$$= \iiint q(\mathbf{X}, \mathbf{S}, \mathbf{f}, \mathbf{U}) \log \left\{ \prod_{i=1}^N \underbrace{\left[\frac{p(\mathbf{y}_i | \mathbf{x}_i)}{p(\mathbf{x}_i | \mathbf{s}_{i-1}, \mathbf{f})} \right]}_{\mathcal{L}_y} \right. \\ \left. \prod_{i=1}^{N-1} \underbrace{\left[\frac{p(\mathbf{s}_i | \mathbf{s}_{i-1}, \mathbf{f})}{q(\mathbf{s}_i)} \right]}_{\mathcal{L}_s} \underbrace{\frac{p(\mathbf{s}_0)}{q(\mathbf{s}_0)}}_{\mathcal{L}_0} \underbrace{\frac{p(\mathbf{f} | \mathbf{U})}{p(\mathbf{f} | \mathbf{U})}}_{\mathcal{L}_f} \underbrace{\frac{p(\mathbf{U})}{q(\mathbf{U})}}_{\mathcal{L}_u} \right\} d\mathbf{X} d\mathbf{S} d\mathbf{f} d\mathbf{U}. \quad (54)$$

Two ratios cancel out, which results the ELBO decomposing into three additive terms

$$\mathcal{L} = \mathcal{L}_y + \mathcal{L}_s + \mathcal{L}_0 + \mathcal{L}_u, \quad (55)$$

where each term contains the (relevant parts of) expectation over $q(\mathbf{X}, \mathbf{S}, \mathbf{f}, \mathbf{U})$.

Likelihood term. The variational likelihood term \mathcal{L}_y is an expectation of the likelihood wrt the variationally marginalized state distributions $q(\mathbf{x}_i)$,

$$\mathcal{L}_y = \iiint q(\mathbf{X}, \mathbf{S}, \mathbf{f}, \mathbf{U}) \log p(\mathbf{Y}|\mathbf{X}) d\mathbf{S} d\mathbf{f} d\mathbf{U} \quad (56)$$

$$= \int q(\mathbf{x}_1) \cdots q(\mathbf{x}_N) \log \prod_{i=1}^N p(\mathbf{y}_i|\mathbf{x}_i) d\mathbf{X} \quad (57)$$

$$= \sum_{i=1}^N \mathbb{E}_{q(\mathbf{x}_i)} \log p(\mathbf{y}_i|\mathbf{x}_i) \quad (58)$$

with marginalized state distributions

$$q(\mathbf{x}_i) = \iiint q(\mathbf{x}_i, \mathbf{s}_{i-1}, \mathbf{f}, \mathbf{U}) d\mathbf{s}_{i-1} d\mathbf{f} d\mathbf{U} \quad (59)$$

$$= \iint p(\mathbf{x}_i|\mathbf{s}_{i-1}, \mathbf{f}) q(\mathbf{s}_{i-1}) q(\mathbf{f}) d\mathbf{s}_{i-1} d\mathbf{f} \quad (60)$$

$$= \int q_{\rightarrow}(\mathbf{x}_i|\mathbf{f}) q(\mathbf{f}) d\mathbf{f} \quad (61)$$

$$= q_{\rightarrow}(\mathbf{x}_i) \quad (62)$$

which are “short” continuous-time normalizing flows $q_{\rightarrow}(\cdot)$ from the previous shooting states $q(\mathbf{s}_{i-1})$ and marginalised over vector fields $q(\mathbf{f})$. We only need samples $\mathbf{x}_i \sim q_{\rightarrow}(\mathbf{x}_i)$ for the Monte Carlo integration of the expected likelihood term. By taking reparameterized samples from the posteriors of the starting point $q(\mathbf{s}_i)$ and the vector field $q(\mathbf{f})$, we can approximate the likelihood term as

$$\mathcal{L}_y \approx \frac{1}{S} \sum_{s=1}^S \sum_{i=1}^N \log p(\mathbf{y}_i|\mathbf{x}_i^{(s)}), \quad (63)$$

where we sum over S reparameterized samples

$$\mathbf{x}_i^{(s)} = \mathbf{s}_{i-1}^{(s)} + \int_{t_{i-1}}^{t_i} \mathbf{f}^{(s)}(\mathbf{s}(\tau)) d\tau, \quad (64)$$

and $\mathbf{f}^{(s)} \sim q(\mathbf{f})$, $\mathbf{s}_{i-1}^{(s)} \sim q(\mathbf{s}_{i-1})$.

Shooting KL term. The shooting term \mathcal{L}_s is a variational expectation over the log ratio between the true shooting state evolution $p_{\rightarrow s}(\mathbf{s}(t_i))$ against the point-wise approximations $q(\mathbf{s}_i)$,

$$\mathcal{L}_s = \iiint q(\mathbf{X}, \mathbf{S}, \mathbf{f}, \mathbf{U}) \log \prod_{i=1}^{N-1} \frac{p(\mathbf{s}_i | \mathbf{s}_{i-1}, \mathbf{f})}{q(\mathbf{s}_i)} d\mathbf{X} d\mathbf{S} d\mathbf{f} d\mathbf{U} \quad (65)$$

$$= \iint q(\mathbf{s}_{N-1}) \cdots q(\mathbf{s}_1) q(\mathbf{s}_0) q(\mathbf{f}) \log \frac{p(\mathbf{s}_{N-1} | \mathbf{s}_{N-2}, \mathbf{f}) \cdots p(\mathbf{s}_1 | \mathbf{s}_0, \mathbf{f})}{q(\mathbf{s}_{N-1}) \cdots q(\mathbf{s}_1)} d\mathbf{S} d\mathbf{f} \quad (66)$$

$$= \sum_{i=1}^{N-1} \left[\iint q(\mathbf{f}) q(\mathbf{s}_i) q(\mathbf{s}_{i-1}) \log p(\mathbf{s}_i | \mathbf{s}_{i-1}, \mathbf{f}) d\mathbf{s}_{i-1} d\mathbf{f} - \int q(\mathbf{s}_i) \log q(\mathbf{s}_i) d\mathbf{s}_i \right] \quad (67)$$

$$= \sum_{i=1}^{N-1} \left[\iint q(\mathbf{f}) q(\mathbf{s}_i) \left(\int q(\mathbf{s}_{i-1}) \log p(\mathbf{s}_i | \mathbf{s}_{i-1}, \mathbf{f}) d\mathbf{s}_{i-1} \right) d\mathbf{s}_i d\mathbf{f} - \int q(\mathbf{s}_i) \log q(\mathbf{s}_i) d\mathbf{s}_i \right] \quad (68)$$

$$= \sum_{i=1}^{N-1} \left[\iint q(\mathbf{f}) q(\mathbf{s}_i) \log q_{\rightarrow}(\mathbf{s}_i | \mathbf{f}) d\mathbf{s}_i d\mathbf{f} - \int q(\mathbf{s}_i) \log q(\mathbf{s}_i) d\mathbf{s}_i \right] \quad (69)$$

$$= \sum_{i=1}^{N-1} \left[\int q(\mathbf{s}_i) \log q_{\rightarrow}(\mathbf{s}_i) d\mathbf{s}_i - \int q(\mathbf{s}_i) \log q(\mathbf{s}_i) d\mathbf{s}_i \right] \quad (70)$$

$$= - \sum_{i=1}^{N-1} \text{KL} [q(\mathbf{s}_i) || q_{\rightarrow}(\mathbf{s}_i)], \quad (71)$$

where the $q_{\rightarrow}(\cdot | \mathbf{f})$ is a change of density of a multivariate Gaussian $q_{i-1}(\mathbf{s}_{i-1})$ through a realization of a non-linear ODE \mathbf{f} in (39), resulting in density of \mathbf{s}_i . We can evaluate this density through the instantaneous change of variables formula (Chen et al., 2018),

$$\log q_{\rightarrow}(\mathbf{s}_i | \mathbf{f}) = \log q_{i-1}(\tilde{\mathbf{s}}_{i-1}) + \int_{t_i}^{t_{i-1}} \text{tr} \left(\frac{\partial \mathbf{f}}{\partial \mathbf{s}(t)} \right) dt \quad (72)$$

$$\tilde{\mathbf{s}}_{i-1} = \mathbf{s}_i + \int_{t_i}^{t_{i-1}} \mathbf{f}(\mathbf{s}(\tau)) d\tau. \quad (73)$$

This procedure entails first integrating $\mathbf{s}_i \sim q(\mathbf{s}_i)$ at time t_i backwards-in-time to find the originating value $\tilde{\mathbf{s}}_{i-1}$ at time t_{i-1} . We can then evaluate the transformed density by computing $q_{i-1}(\tilde{\mathbf{s}}_{i-1})$ and adjusting it with the density change.

Equivalently, we can compute the above term by doing the following forward integration

$$\log q_{\rightarrow}(\mathbf{s}_i | \mathbf{f}) = \log q_i(\tilde{\mathbf{s}}_i) + \int_{t_{i-1}}^{t_i} \text{tr} \left(\frac{\partial \mathbf{f}}{\partial \mathbf{s}(t)} \right) dt \quad (74)$$

$$\tilde{\mathbf{s}}_i = \mathbf{s}_{i-1} + \int_{t_{i-1}}^{t_i} \mathbf{f}(\mathbf{s}(\tau)) d\tau. \quad (75)$$

In this procedure, we first sample the originating value $\mathbf{s}_{i-1} \sim q(\mathbf{s}_{i-1})$ at time t_{i-1} and solve the system forward-in-time to generate $\tilde{\mathbf{s}}_i$ at time t_i . We then evaluate the transformed density by computing $q_i(\tilde{\mathbf{s}}_i)$ at time t_i and adjusting it with the density change term. This is more efficient in practice, since it avoids the additional backward ODE solve.

The shooting KL term (71) can be decomposed a cross-entropy term an entropy term (70). The cross-entropy term involves the continuous-time normalizing flow and can be evaluated with Monte Carlo

integration. The entropy term can be simplified analytically as entropy of multivariate Gaussians.

$$\mathcal{L}_s = - \sum_{i=1}^{N-1} \text{KL} [q(\mathbf{s}_i) || q_{\rightarrow}(\mathbf{s}_i)] \quad (76)$$

$$= \sum_{i=1}^{N-1} \left[\int q(\mathbf{s}_i) \log q_{\rightarrow}(\mathbf{s}_i) d\mathbf{s}_i - \int q(\mathbf{s}_i) \log q(\mathbf{s}_i) d\mathbf{s}_i \right] \quad (77)$$

$$\approx \sum_{i=1}^{N-1} \left[\frac{1}{S} \sum_{s=1}^S \log q_{\rightarrow}(\mathbf{s}_i^{(s)} | \mathbf{f}^{(s)}) - \int q(\mathbf{s}_i) \log q(\mathbf{s}_i) d\mathbf{s}_i \right] \quad (78)$$

$$(79)$$

where we take S reparameterized samples $\mathbf{s}_i^{(s)} \sim q(\mathbf{s}_i)$ and $\mathbf{f}^{(s)} \sim q(\mathbf{f})$.

Initial state KL. This term corresponds to the KL divergence between variational posterior and the prior distribution of the initial state. With the assumption of Gaussian prior and variational posterior, this term can also be derived analytically,

$$\mathcal{L}_0 = \int q(\mathbf{s}_0) \log \frac{p(\mathbf{s}_0)}{q(\mathbf{s}_0)} d\mathbf{s}_0 \quad (80)$$

$$= - \text{KL} [q(\mathbf{s}_0) || p(\mathbf{s}_0)] \quad (81)$$

Inducing KL. This term corresponds to the KL divergence between variational posterior and prior distribution of inducing values. This term can also be derived analytically as the KL between multivariate Gaussians.

$$\mathcal{L}_u = \int q(\mathbf{U}) \log \frac{p(\mathbf{U})}{q(\mathbf{U})} d\mathbf{U} \quad (82)$$

$$= \sum_{d=1}^D \int q(\mathbf{u}_d) \log \frac{p(\mathbf{u}_d)}{q(\mathbf{u}_d)} d\mathbf{u} \quad (83)$$

$$= - \sum_{d=1}^D \text{KL} [q(\mathbf{u}_d) || p(\mathbf{u}_d)] \quad (84)$$

Complete ELBO. The full ELBO is then

$$\mathcal{L} = \sum_{i=1}^N \mathbb{E}_{q_{\rightarrow}(\mathbf{x}_i)} \log p(\mathbf{y}_i | \mathbf{x}_i) - \sum_{i=1}^{N-1} \text{KL} [q(\mathbf{s}_i) || q_{\rightarrow}(\mathbf{s}_i)] \quad (85)$$

$$- \text{KL}[q(\mathbf{s}_0) || p(\mathbf{s}_0)] - \text{KL}[q(\mathbf{u}) || p(\mathbf{u})] \quad (86)$$

Experiments

Optimization setup

We use Adam (Kingma and Ba, 2014) optimizer and jointly train all the variational parameters and hyperparameters. The complete list of optimized parameters, along with additional method-specific details, are given below.

Vanilla GPODE model. We use ‘whitened’ representation for inducing variables and optimize following parameters against the evidence lowerbound.

- Variational posterior parameters for inducing variables $q(\mathbf{U})$ and initial states $q(\mathbf{x}_0)$ - mean and covariance parameters of the Gaussian approximation.
- Inducing locations \mathbf{Z} .
- Likelihood parameters - noise variance parameter in case of Gaussian likelihood.
- Kernel parameters - lengthscales and signal variance parameters in case of squared exponential kernel.

Shooting GPODE model. We use ‘whitened’ representation for inducing variables and optimize the following parameters against the evidence lower bound.

- Variational posterior parameters for inducing variables $q(\mathbf{U})$ and shooting states $q(\mathbf{S})$ - mean and covariance parameters of the Gaussian approximation.
- Inducing locations \mathbf{Z} .
- Likelihood parameters - noise variance parameter in case of Gaussian likelihood.
- Kernel parameters - length scales and signal variance parameters in case of the squared exponential kernel.

npODE model. We use ‘whitened’ representation for inducing variables, maximum a posteriori (MAP) objective, and optimize following parameters:

- Inducing values \mathbf{U} and locations \mathbf{Z} .
- Likelihood parameters - noise variance parameter in case of Gaussian likelihood.
- Kernel parameters - length scales and signal variance parameters in case of the squared exponential kernel.

NeuralODE model. We use \tanh activation and a fully connected block with one hidden layer having 32 units in Van der Pol/ Fitz-Hugh Nagumo experiments and 64 hidden units in CMU MoCap experiments. All the network parameters were optimized against L1 loss.

Gradient initialization strategy

In case of sparse Gaussian process model with inducing variables, we initialize the vector field with empirical gradients from the observed data. We first initialize inducing locations \mathbf{Z} as `kmeans` cluster centers of observations \mathbf{Y} . Next we compute empirical gradient estimates, $\dot{\mathbf{Y}} = (\mathbf{y}_2 - \mathbf{y}_1, \mathbf{y}_3 - \mathbf{y}_2, \dots, \mathbf{y}_N - \mathbf{y}_{N-1})$ at locations $\tilde{\mathbf{Y}} = (\mathbf{y}_1, \mathbf{y}_2, \dots, \mathbf{y}_{N-1})$ and initialize inducing values \mathbf{U} as the GP mean interpolation of empirical gradients at inducing locations.

$$\mathbf{U} = \Delta t \cdot K(\mathbf{Z}, \tilde{\mathbf{Y}}) K(\tilde{\mathbf{Y}}, \tilde{\mathbf{Y}})^{-1} \dot{\mathbf{Y}}, \quad (87)$$

where Δt is the time difference between two consecutive observations in the dataset.

CMU MoCap dataset

The dataset used in this experiment was obtained from <http://mocap.cs.cmu.edu/>. The database consists of sensor recordings for different activities in .amc files. We use data for three subjects 09, 35, and 39. The action sequences considered for train, validation and test purposes are given in table 1. The training sequences and their lengths were selected to include at least one full cycle of the dynamics while learning the model.

(a) subject	(b) activity	(c) split	(d) # sequences	(e) files
subject 09	running	train	6	05.amc, 06.amc, 07.amc, 08.amc, 09.amc, 11.amc
		validation	2	01.amc, 02.amc
		test	2	03.amc, 04.amc
subject 35	walking	train	16	01.amc, 02.amc, 03.amc, 04.amc, 05.amc, 06.amc, 07.amc, 08.amc, 09.amc, 10.amc, 11.amc, 12.amc, 13.amc, 14.amc, 15.amc, 16.amc
		validation	3	28.amc, 29.amc, 30.amc
		test	4	31.amc, 32.amc, 33.amc, 34.amc
subject 39	walking	train	6	01.amc, 02.amc, 07.amc, 08.amc, 09.amc, 10.amc
		validation	2	03.amc, 04.amc
		test	2	05.amc, 06.amc

Table 1: For each subject (a), we report the activity considered for the experiment (b), the data split train/validation/test (c), the number of sequences considered for the corresponding split (d), and the files used in the corresponding split (e).

(a) subject	(b) experiment	(c) split	(d) sequence length
subject 09	short	train	50
		validation	120
		test	120
	long	train	100
		validation	120
		test	120
subject 35	short	train	50
		validation	300
		test	300
	long	train	250
		validation	300
		test	300
subject 39	short	train	100
		validation	300
		test	300
	long	train	250
		validation	300
		test	300

Table 2: For each subject (a), we report the experiment type (b), the data split train/validation/test (c), and the number of observations considered for the corresponding split.